Journal of
Applied
Crystallography

ISSN 1600-5767

Received 15 July 2013
Accepted 27 March 2014

Analysis of crystalline perfection of pure and Mo-doped KTP crystals on different growth planes by high-resolution X-ray diffraction

Jayavelu Rajeev Gandhi,[a] Muthian Rathnakumari,[a] Pandarinathan Muralimanohar,[a] Palanivel Sureshkumar[a]* and Godavarthi Bhagavannarayana[b]

[a]Materials Research Centre, Department of Physics, Velammal Engineering College, Chennai 600066, India, and [b]Crystal Growth and X-ray Analysis, National Physics Laboratory (CSIR), New Delhi 110012, India. Correspondence e-mail: suresrath@yahoo.com

Single crystals of pure and molybdenum (Mo)-doped potassium titanyl phosphate (KTP) crystals were grown by the high-temperature solution growth technique. The presence of dopant ions in the grown crystal was confirmed by energy-dispersive X-ray analysis. Grown crystals, cut along various growth planes such as (100), (011) or (201), were analysed for crystalline perfection using high-resolution X-ray diffraction (HRXRD). Although the HRXRD study showed that the crystalline perfection of most of the crystals was quite good without any structural defects, structural grain boundaries were observed in some of the crystals chosen for study. The observed structural defects are probably due to mechanical or thermal fluctuations occurring during the growth process.

1. Introduction

Potassium titanyl phosphate (KTP) is an efficient nonlinear optical crystal suitable for various frequency-conversion applications, particularly for frequency doubling of lasers at wavelengths near 1 μm (Chuang *et al.*, 1994; Bierlein & Vanherzeele, 1989). The efficient operation of KTP optical parametric oscillators pumped by multimode Nd:YLF (yttrium lithium fluoride) and Nd:YAG (yttrium aluminum garnet) lasers has also been demonstrated (Rines *et al.*, 1994). Its high nonlinear optical coefficients, high optical damage threshold, wide acceptance angles, high thermal and mechanical stability, non-hygroscopicity, large linear electro-optic coefficients and low dielectric constants make it useful for various electro-optic applications (Bierlein & Arweiler, 1986).

Generally two main techniques, namely hydrothermal and flux techniques, are used for the growth of KTP crystals (Zhang *et al.*, 2006; Roth & Tseitlin, 2010; Wang *et al.*, 2009). The hydrothermal process requires high temperatures (of the order of 773 K) and pressure (of the order of 1360 bar; 1 bar = 100 000 Pa) and the growth rate of KTP crystals is very low (Bierlein & Vanherzeele, 1989; Laudise *et al.*, 1986). Large single crystals of KTP are mostly grown by the flux technique and this is the most popular method. The significant advantage of using the flux process is that it operates at atmospheric pressure and hence does not require sophisticated pressure equipment, and it is easy to design scaled-up furnaces. The quality and external morphology of KTP crystals grown by the flux technique depend on many parameters, such as initial chemical composition, growth temperature, supersaturation around the nuclei, position of the crystal in the crucible, hydrodynamic conditions, defect content in the crystal *etc.* (Satyanarayan & Bhat, 1997; Dhanaraj & Bhat, 1990; Wang *et al.*, 2009).

Doping is a useful means of modifying the properties of crystals. Shi *et al.* (1999) and Zaldo *et al.* (1999) have reported the effect of impurities and defects, particularly on the optical and structural aspects of KTP crystals. The quality of large KTP crystals can be characterized by X-ray topography using characteristic X-ray radiation and synchrotron white radiation (Bolt *et al.*, 1991; Halfpenny *et al.*, 1991; Stolzenberger, 1988).

High-resolution X-ray diffraction (HRXRD) is one of the most widely used techniques for determining crystalline perfection and for defect studies of single crystals. Evaluation of crystalline perfection is very important, particularly when the crystals are doped, as these dopants influence the crystalline perfection; this is especially true at higher concentrations and for larger-sized crystals (Bhagavannarayana *et al.*, 2008). In the present investigation we have grown pure and Mo-doped KTP crystals by the flux technique and have analysed their crystalline perfection on different growth planes using HRXRD.

2. Experimental details

2.1. Synthesis and crystal growth

Single crystals of pure and Mo-doped KTP were grown by the spontaneous nucleation technique from a K_6 self-flux (Godfrey, 1991). The starting materials, potassium dihydrogen orthophosphate (KH_2PO_4), dipotassium hydrogen orthophosphate (K_2HPO_4) and titanium dioxide (TiO_2), were

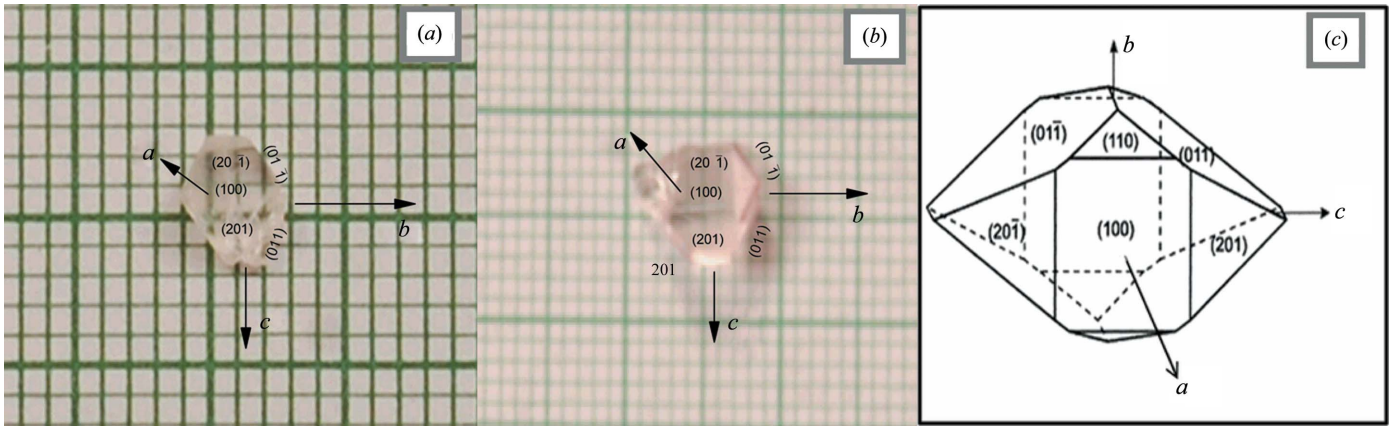

Figure 1
As-grown crystals of (*a*) pure KTP and (*b*) Mo-doped KTP. (*c*) Typical crystal morphology.

weighed (31.4654 g of KH_2PO_4, 18.5871 g of K_2HPO_4 and 9.9473 g of TiO_2) and added directly to a platinum crucible. The initial compounds were prepared by taking KTP and flux $K_6P_4O_{13}$ (K_6) in the ratio of 7:3 as per the following reactions:

$$6KH_2PO_4 + 6K_2HPO_4 \rightarrow 3K_6P_4O_{13} + 9H_2O,$$

$$7KH_2PO_4 + 7TiO_2 \rightarrow 7KTiOPO_4 + 7H_2O.$$

A charge of 60 g of the initial compounds was loaded into a 50 ml platinum crucible, which was mounted in a double-zone resistance furnace with a vertical temperature gradient in each zone of about ± 2 K cm^{-1}. The temperature of the furnace was increased from room temperature to 1323 K and maintained for 30 h, with constant stirring of the sample by a platinum rod for complete homogenization. After homogenization, the saturated solution was cooled to room temperature at different cooling rates, as reported in our earlier work (Rajeev Gandhi *et al.*, 2011; Rathnakumari *et al.*, 2013). The process of nucleation began at 1253 K and continued down to 1173 K. A cooling rate of 0.5 K h^{-1} was maintained down to 1173 K and thereafter a rate of 25 K h^{-1} until the sample reached room temperature. After the growth process, good quality crystals were harvested from the solidified flux. For the growth of Mo-doped KTP crystals, 0.005 mol% of MoO_3 was added to the starting materials. Fig. 1 shows the grown colourless pure (Fig. 1*a*) and violet-tinted Mo-doped (Fig. 1*b*) KTP crystals, along with the reported crystal morphology (Fig. 1*c*), showing the (100), (011), (01$\bar{1}$), (201), (20$\bar{1}$) and (110) faces (Solé *et al.*, 1996; Roth *et al.*, 2001).

Crystals exhibiting the natural crystal habits of KTP with well developed facets were selected, cut in different orientations and polished. Figs. 2(*a*) and 2(*b*) show the cut and polished samples of pure and Mo-doped KTP crystals, respectively.

3. Characterization

The elemental composition of the samples was determined by energy dispersive X-ray analysis (EDX) using a JEOL JFM6390 scanning electron microscope. The crystalline perfection of the grown single crystals was characterized by HRXRD using a multicrystal X-ray diffractometer developed at NPL (Lal & Bhagavannarayana, 1989).

4. Results and discussion

4.1. EDX analysis

In order to confirm the chemical compositions of the pure and Mo-doped KTP crystals, the samples were subjected to EDX as described above. From the EDX spectra, the presence

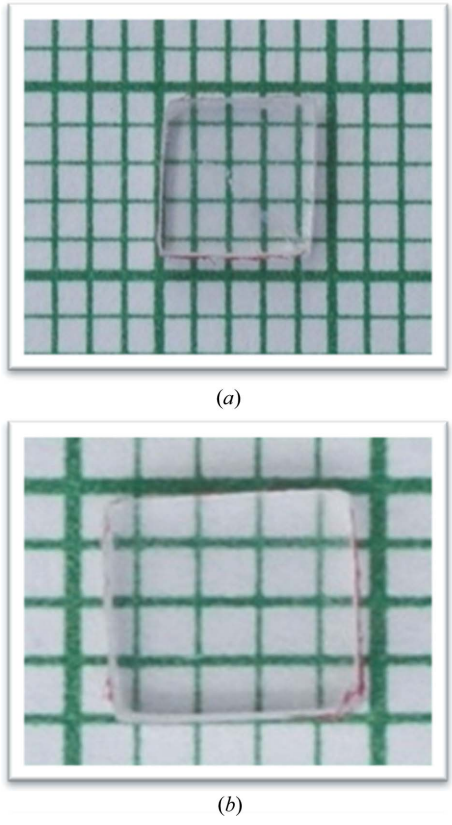

Figure 2
Cut and polished crystals of (*a*) pure KTP and (*b*) Mo-doped KTP.

of Mo in the doped KTP crystals was confirmed, and the concentration was found to be 0.07 at.% in the grown crystals.

4.2. High-resolution X-ray diffractometry

The crystalline perfection of the grown single crystals was characterized by HRXRD using a multicrystal X-ray diffractometer as described above. The well collimated and monochromated Mo $K\alpha_1$ beam obtained from three monochromator Si crystals set in a dispersive (+,−,−) configuration was used as the incident X-ray beam. The specimen crystal was aligned in the (+,−,−,+) configuration. As a result of the dispersive configuration, although the lattice constants of the monochromator crystal(s) and the specimen are different, the unwanted dispersion broadening in the diffraction curve (DC) of the specimen crystal is insignificant. The specimen can be rotated about the vertical axis, which is perpendicular to the plane of diffraction, with a minimum angular interval of 0.4″. Rocking or diffraction curves were recorded by changing the glancing angle (the angle between the incident X-ray beam and the surface of the specimen) around the Bragg diffraction peak position θ_B (taken as zero for the sake of convenience), starting from a suitable arbitrary glancing angle and ending at a glancing angle after the peak, so that all the meaningful scattered intensities on both sides of the peak are included in the DC. The DC was recorded by the so-called ω scan, wherein the detector was kept at the same angular position $2\theta_B$ with a wide opening for its slit. This arrangement is particularly appropriate for recording the short-range-order scattering caused by defects, the scattering from local Bragg diffractions from agglomerated point defects, or the scattering due to low-angle and very low angle structural grain boundaries (Bhagavannarayana & Kushwaha, 2010; Senthil Kumar *et al.*, 2011).

Before recording the DC, the specimen was first lapped and chemically etched in a nonpreferential etchant in order to remove any noncrystallized solute atoms remaining on the surface of the crystal and the possible layer that may sometimes form on the surface of crystals grown by solution methods (Bhagavannarayana *et al.*, 2006), and also to ensure surface planarity.

To obtain more understanding about HRXRD, it may be mentioned here that the technique follows the dynamic theory which takes into account all interactions between scattered waves from all irradiated atoms. Any atom/unit cell inside the crystal receives scattered waves from all other atoms/unit cells in addition to the incident beam. Thus, the resultant wavefield inside the crystal is unique and the diffracted beam carries information about the deviation of the bulk crystal from periodicity or order. As the X-ray beam penetrates several micrometres inside the crystal, the DC pertaining to a particular set of planes is a true representative of the overall level of perfection of the whole bulk crystal in a broad perspective. However, some defects, like grain boundaries, as in the present case, or dislocations, are orientation specific, and then one may obtain more specific information about such defects by recording DCs for a specific set of (*hkl*) planes (Riscob *et al.*, 2012).

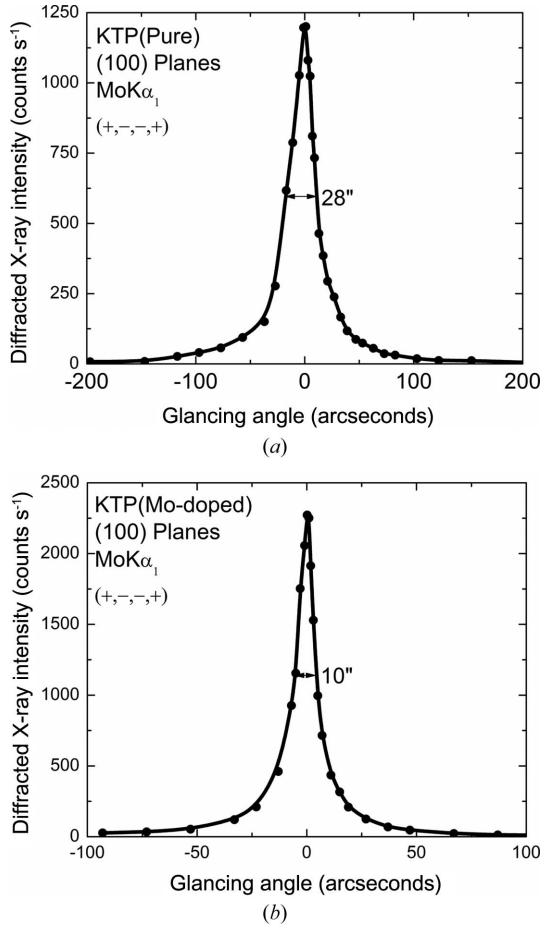

Figure 3
High-resolution X-ray DCs recorded for typical (*a*) pure KTP and (*b*) Mo-doped KTP single crystals, using the (100) diffracting planes in a symmetrical Bragg geometry with Mo $K\alpha_1$ radiation.

4.2.1. Pure and Mo-doped KTP: the (100) diffraction plane. Fig. 3 shows the high-resolution DCs recorded for typical pure KTP (Fig. 3*a*) and Mo-doped KTP (Fig. 3*b*) specimens grown by the flux method using the (100) diffracting planes in a symmetrical Bragg geometry employing the multicrystal X-ray diffractometer with Mo $K\alpha_1$ radiation. As seen in the figure, the DCs are quite sharp, without any satellite peaks which may otherwise be observed either because of internal structural grain boundaries (Bhagavannarayana *et al.*, 2005) or because of the epitaxial layer that may sometimes form in crystals grown from solution (Bhagavannarayana *et al.*, 2006). For pure KTP, the full width at half-maximum (FWHM) of the DC is 28″, while for Mo:KTP the FWHM of the DC is 10″, which is very close to the value expected from the plane-wave theory of dynamic X-ray diffraction (Betterman & Cole, 1964). These single sharp DCs with very low FWHMs indicate that the crystalline perfection is quite good with no internal structural grain boundaries.

4.2.2. Pure and Mo-doped KTP: the (011) diffraction plane. Fig. 4 shows the high-resolution X-ray DCs recorded for the (011) diffraction planes using Mo $K\alpha_1$ radiation for typical

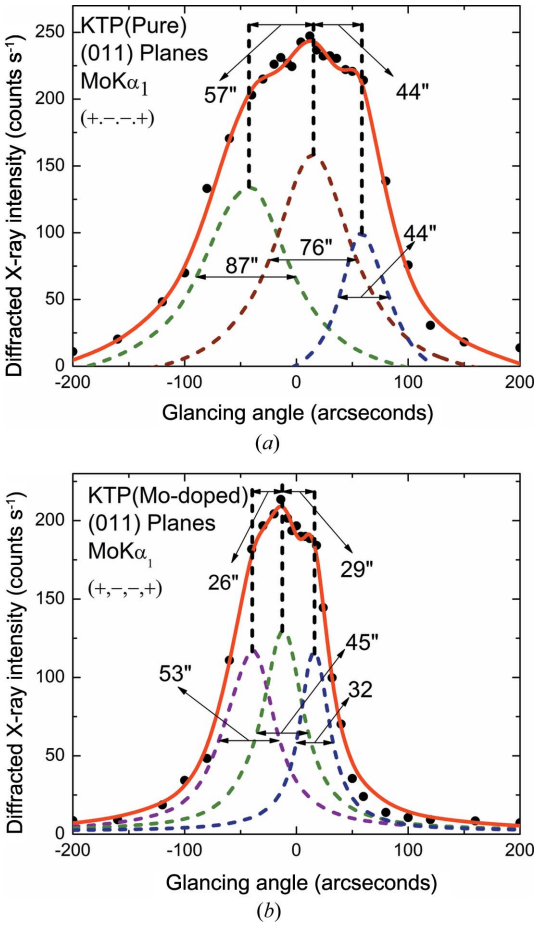

Figure 4
High-resolution X-ray DCs recorded for typical (*a*) pure KTP and (*b*) Mo-doped KTP single crystals, using the (011) diffracting planes in a symmetrical Bragg geometry with Mo $K\alpha_1$ radiation.

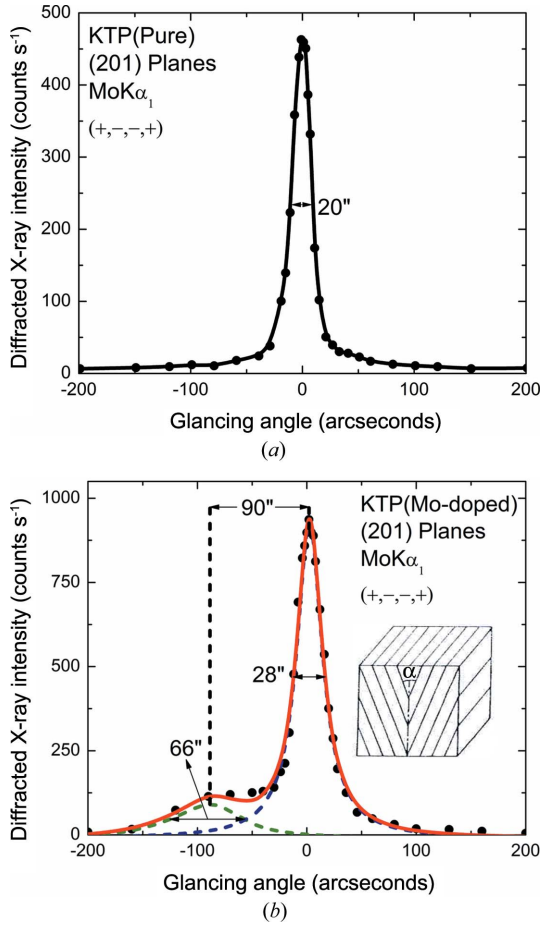

Figure 5
High-resolution X-ray DCs recorded for typical (*a*) pure KTP and (*b*) Mo-doped KTP single crystals, using the (201) diffracting planes in a symmetrical Bragg geometry with Mo $K\alpha_1$ radiation.

pure KTP (Fig. 4*a*) and Mo-doped KTP (Fig. 4*b*) single-crystal specimens. On close observation one can realize that the curves are not single peaks. On deconvolution of the DCs, it is clear that these curves contain two additional peaks. The solid line (convoluted curve) is well fitted with the experimental points represented by filled circles, which are 57 and 44″ away from the central peak on both sides for pure KTP, and 26 and 29″ away for Mo:KTP. These two additional peaks correspond to two very low angle internal structural boundaries (tilt angle > 1′ but < 1°; Bhagavannarayana *et al.*, 2005) whose tilt angles (which may be defined as the misorientation angle between the two crystalline regions on either side of a structural grain boundary) are 57 and 44″ for pure KTP, and 26 and 29″ for Mo:KTP, from their adjoining regions. The FWHMs of the central peaks and the two very low angle boundaries are, respectively, 76, 87 and 44 ″ for pure KTP, and 45, 53 and 32″ for Mo:KTP. The relatively low values of the FWHMs of the grains compared with those of good crystals (which are of the order of a few arcseconds; Senthil Kumar *et al.*, 2011) indicate that the crystalline perfection is quite good.

4.2.3. Pure and Mo-doped KTP: the (201) diffraction plane. Fig. 5 shows the high-resolution DCs recorded for typical pure KTP (Fig. 5*a*) and Mo-doped KTP (Fig. 5*b*) specimen crystals grown by the flux method using the (201) diffracting planes in a symmetrical Bragg geometry employing the multicrystal X-ray diffractometer with Mo $K\alpha_1$ radiation. As seen in Fig. 5(*a*), the DC is quite sharp without any satellite peaks, and the FWHM of the DC is 20″. This single sharp DC with very low FWHM indicates that the crystalline perfection is quite good with no internal structural grain boundaries.

As seen in Fig. 5(*b*), one can see that the curve is not a single peak. On deconvolution of the DC, it is clear that the curve contains an additional peak 90″ away from the main peak. This additional peak corresponds to a low-angle internal structural boundary. For a better understanding, a schematic of the structural grain boundary is given in the inset of Fig. 5(*b*), where α denotes the tilt angle, *i.e.* the angular separation between the two peaks; α = 90″ in the specimen crystal shown in the inset. Further details of such structural grain boundaries, including their effect on physical properties, are available elsewhere (Bhagavannarayana & Kushwaha, 2010; Bhagavannarayana *et al.*, 2005). The FWHMs of the main peak and the low-angle boundary are 28 and 66″, respectively. These low FWHM values and the low angular spread (∼200″) of the DC indicate that the crystalline perfection is quite good.

These types of structural defect (as also seen in Fig. 4) are probably generated in the crystals as a result of mechanical or thermal fluctuations occurring during the growth process or doping, or they may be due to fast growth (Bhagavannarayana *et al.*, 2010). As it is well known that crystal growth is very sensitive to mechanical disturbances, including very small disturbances that may be caused by natural processes inside the Earth or even when one walks in the vicinity of crystal growth vessels, such mechanical disturbances may disturb the growth process, leading to structural defects. Defects may also be generated by very small thermal fluctuations in the growth vessel. These are unavoidable most of the time but can cause such defects.

It may be mentioned here that such minute defects can be detected from the well resolved peaks in the DCs only because of the high resolution of the diffractometer, characterized by very low values of the wavelength spread $\Delta\lambda/\lambda$ and of the horizontal divergence for the incident beam, which are around 10^{-5} and much less than $3''$, respectively, for the multicrystal X-ray diffractometer used in the present studies. Such defects may not have much impact on the physical properties. However, a quantitative analysis of such unavoidable defects is of great importance, particularly in the case of phase-matching applications of nonlinear optical crystals, as explained in our recent article (Bhagavannarayana *et al.*, 2011).

5. Conclusion

Pure and Mo-doped KTP crystals were grown by the spontaneous nucleation method using a K_6 flux. EDX confirmed the presence of Mo ions in the doped samples. The degree of crystalline perfection was evaluated on different growth planes of the pure and doped crystals using HRXRD. Structural defects and grain boundaries were observed in some of the growth planes, which may be due to mechanical or thermal fluctuations occurring during the growth process. The study of such unavoidable defects is of great importance, particularly in the case of phase-matching applications.

The authors thank the DRDO for a research grant (No. ERIP/ER/0504330/M/01/917). We also thank Dr V. Sridharan, CMPD, XCGS (IGCAR), Kalpakkam, for cutting the crystals in the required orientations.

References

Betterman, B. W. & Cole, H. (1964). *Rev. Mod. Phys.* **36**, 681–717.
Bhagavannarayana, G., Ananthamurthy, R. V., Budakoti, G. C., Kumar, B. & Bartwal, K. S. (2005). *J. Appl. Cryst.* **38**, 768–771.
Bhagavannarayana, G. & Kushwaha, S. K. (2010). *J. Appl. Cryst.* **43**, 154–162.
Bhagavannarayana, G., Parthiban, S. & Meenakshisundaram, S. (2006). *J. Appl. Cryst.* **39**, 784–790.
Bhagavannarayana, G., Parthiban, S. & Meenakshisundaram, S. (2008). *Cryst. Growth Des.* **8**, 446–451.
Bhagavannarayana, G., Rajesh, P. & Ramasamy, P. (2010). *J. Appl. Cryst.* **43**, 1372–1376.
Bhagavannarayana, G., Riscob, B. & Shakir, M. (2011). *Mater. Chem. Phys.* **126**, 20–23.
Bierlein, J. D. & Arweiler, C. B. (1986). *Appl. Phys. Lett.* **49**, 917–919.
Bierlein, J. D. & Vanherzeele, H. (1989). *J. Opt. Soc. Am. B*, **6**, 622–633.
Bolt, R. J., de Haas, H., Sebastian, M. T. & Klapper, H. (1991). *J. Cryst. Growth*, **110**, 587–594.
Chuang, T., Hays, A. D. & Verdun, H. R. (1994). *Adv. Solid State Lasers*, **20**, 314–318.
Dhanaraj, G. & Bhat, H. L. (1990). *Mater. Lett.* **10**, 283–287.
Godfrey, K. W. (1991). *Mater. Sci. Eng. B*, **9**, 479–483.
Halfpenny, P. J., O'Neill, L., Sherwood, J. N., Simpson, G. S., Yokotani, A., Miyamoto, A., Sasaki, T. & Nakai, S. (1991). *J. Cryst. Growth*, **113**, 722–725.
Lal, K. & Bhagavannarayana, G. (1989). *J. Appl. Cryst.* **22**, 209–215.
Laudise, R. A., Cava, R. J. & Caporaso, A. J. (1986). *J. Cryst. Growth*, **74**, 275–280.
Rajeev Gandhi, J., Vijayalakshmi, B., Rathnakumari, M. & Sureshkumar, P. (2011). *J. Miner. Mater. Charact. Eng.* **10**, 683–691.
Rathnakumari, M., Rajeev Gandhi, J., Manohar, P. M. & Sureshkumar, P. (2013). *Optik*, **124**, 5702–5706.
Rines, G. A., Rhes, D. M. & Moulton, P. F. (1994). *Adv. Solid State Lasers*, **20**, 461–463.
Riscob, B., Shakir, M., Vijayan, N., Maurya, K. K., Wahab, M. A. & Bhagavannarayana, G. (2012). *J. Appl. Cryst.* **45**, 679–685.
Roth, M., Angert, N., Tseitlin, M. & Alexandrovski, A. (2001). *Opt. Mater.* **16**, 131–136.
Roth, M. & Tseitlin, M. (2010). *J. Cryst. Growth*, **312**, 1059–1064.
Satyanarayan, M. N. & Bhat, H. L. (1997). *J. Cryst. Growth*, **181**, 281–289.
Senthil Kumar, K., Moorthy Babu, S. & Bhagavannarayana, G. (2011). *J. Appl. Cryst.* **44**, 313–318.
Shi, L.-P., Chong, T.-C. & Xu, X.-W. (1999). *J. Cryst. Growth*, **198**, 551–554.
Solé, R., Ruiz, X., Cabré, R., Gavaldà, J., Aguiló, M., Díaz, F., Nikolov, V. & Solans, X. (1996). *J. Cryst. Growth*, **167**, 681–685.
Stolzenberger, R. A. (1988). *Appl. Opt.* **27**, 3883–3886.
Wang, J., Zhang, H., Jiang, M., Nikitina, M., Maltsev, V. & Leonyu, N. (2009). *Cryst. Growth Des.* **9**, 1190–1193.
Zaldo, C., Rico, M., Díaz, F. & Carvajal, J. (1999). *Opt. Mater.* **13**, 175–180.
Zhang, C.-L., Huang, L.-X., Zhou, W.-N., Zhang, G., Hou, H.-D., Ruan, Q.-F., Lei, W., Qin, S.-J., Lu, F.-H., Zuo, Y.-B., Shen, H.-Y. & Wang, G.-F. (2006). *J. Cryst. Growth*, **292**, 364–367.